ChemComm

COMMUNICATION

View Article Online
View Journal

Cite this: DOI: 10.1039/c5cc00534e

Received 19th January 2015,
Accepted 19th February 2015

DOI: 10.1039/c5cc00534e

www.rsc.org/chemcomm

Ionic liquid-mediated synthesis of meso-scale porous lanthanum-transition-metal perovskites with high CO oxidation performance†

Hanfeng Lu,*[ab] Pengfei Zhang,[b] Zhen-An Qiao,[b] Jinshui Zhang,[b] Huiyuan Zhu,[b] Jihua Chen,[c] Yinfei Chen[a] and Sheng Dai*[bd]

Lanthanum-transition-metal perovskites with robust meso-scale porous frameworks (meso-$LaMO_3$) are synthesized through the use of ionic liquids. The resultant samples demonstrate a rather high activity for CO oxidation, by taking advantage of unique nanostructure-derived benefits. This synthesis strategy opens up a new opportunity for preparing functional mesoporous complex oxides of various compositions.

Lanthanum transition metal perovskites ($LaMO_3$, M = Mn, Fe, Co, Ni) are highly attractive for many applications—including catalysis,[1] chemical sensors,[2] solid oxide fuel cells,[3] and pseudo-capacitors[4]—because of their unique physicochemical and electronic properties such as redox potential, ion mobility, semiconductive electronic structure, and rather high thermal stability.[5] There are many well-established synthetic protocols for $LaMO_3$ preparation, for example, co-precipitation,[6] citrate sol–gel,[7] and mechanosynthesis.[8] However, the samples derived from such synthetic methods are bulk materials with relatively low surface areas (<10 m^2 g^{-1}), which greatly restrict their performance in target applications, particularly heterogeneous catalysis. The incorporation of mesopores in bulk $LaMO_3$ therefore is regarded as an ideal solution to address the above issue. Textural engineering of metal oxides with an accessible meso-scale porous framework would, in principle, not only facilitate mass transfer but also provide more catalytic sites for surface reactions.[9] Toward this end, meso-scale porous $LaMO_3$ samples (meso-$LaMO_3$) with different morphologies have been successfully synthesized with the aid of sacrificial hard templates (for example, mesoporous silica).[10] However, the removal of the hard templates often presents serious safety problems because they require the use of toxic reagents such as HF and NaOH.[11] In addition, the strong host–guest interaction induced by the crystallization of $LaMO_3$ perovskite at elevated temperatures often results in incomplete removal of parent templates, making the synthesis of template-free $LaMO_3$ difficult.[12] Hence it is highly desirable to develop an alternative synthetic strategy for meso-$LaMO_3$ fabrication.

Evaporation-induced self-assembly (EISA) was considered to be a highly efficient protocol for the synthesis of mesoporous metal oxides and their mixed oxides.[13] However, organic surfactants used in EISA, such as CTAB (cetyl trimethylammonium bromide) and P123 (tri-block copolymer), always decompose before they crosslink well with metal-containing species, owing to their low thermal stability. This instability issue associated with the current soft templates often results in an unstable mesoporous framework that easily collapses during crystallization of perovskite at an elevated temperature.[14] In this regard, an excellent thermally stable template with abundant anchoring sites for metal species coordination is therefore highly desirable for the construction of mesoporous $LaMO_3$ at an elevated temperature. Recently, room temperature ionic liquids with rather high thermal stability have been extensively used as the porosity-directing agents for the preparation of carbon,[15] zeolites,[16] SiO_2[17] and TiO_2[18] based nanoarchitectures, greatly outstanding the development of nanochemistry.[19] By considering their supermolecule-like properties with rich hydrogen bonding networks, strong electrostatic interaction and good stability,[20] these kinds of ionic liquids chemically should also function as promising media for the synthesis of meso-$LaMO_3$ perovskites.

Herein, ionic liquids with good thermal stability against water and air were employed as soft media for nanostructural engineering of $LaMO_3$ perovskites with robust mesoporous frameworks *via* an enhanced electrostatic $S^+X^-I^+$ self-assembly

[a] *Institute of Catalytic Reaction Engineering, College of Chemical Engineering, Zhejiang University of Technology, Hangzhou, 310014, China. E-mail: luhf@zjut.edu.cn; Fax: +86 0571 88320767; Tel: +86 0571 88320767*
[b] *Chemical Sciences Division, Oak Ridge National Laboratory, Oak Ridge, Tennessee 37831, USA. E-mail: dais@ornl.gov*
[c] *Center for Nanophase Materials Sciences and Chemical Science Division, Oak Ridge National Laboratory, USA*
[d] *Department of Chemistry, University of Tennessee, Knoxville, Tennessee, 37996, USA*

† Electronic supplementary information (ESI) available: A detailed description of the experimental procedure and characterization results. See DOI: 10.1039/c5cc00534e

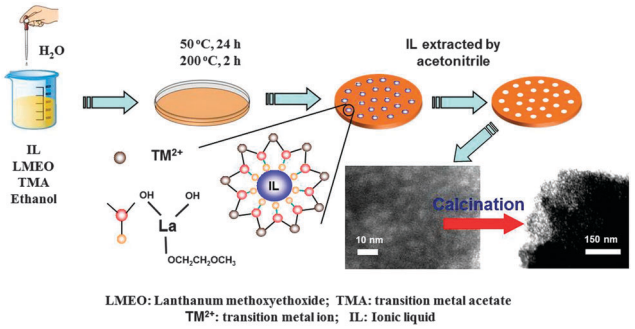

Scheme 1 The synthesis process of mesoporous lanthanum transition metal perovskite oxides by an ionic liquid.

approach. In Scheme 1, lanthanum methoxyethoxide (LMEO) and a transition metal acetate were used as the precursors of lanthanum, and the transition metal (M) and the cation (S^+) and the anion (X^-) of selected ionic liquids directly mediated the assembly of lanthanum and M inorganic species (I^+). Lanthanum and M in nanodomains easily achieve the stoichiometric ligand of the precursors. From the viewpoint of reaction dynamics, the stoichiometric ligand of the reaction reagents in nanodomains not only promotes the formation of $LaMO_3$ perovskites after heating but, more importantly, is beneficial for the construction of robust mesoporous frameworks. In addition, ionic liquids with molecular sizes ranging from 1 to 10 nm, should self-function as soft templates for meso-phase structure generation, making the pore size highly tunable. After being well aged in a high-temperature condition for further crosslinking, the ionic liquids can be extracted completely by acetonitrile and recycled in another new synthetic process (Fig. S1, ESI†). The resultant nanocomposite film is further heated at an elevated temperature to induce the formation of $LaMO_3$ perovskites. Experimentally, four kinds of $LaMO_3$ (M = Mn, Fe, Co, and Ni) perovskites were mediated by the ionic liquid $[Bmim]^+Tf_2N^-$. See ESI† for detailed synthetic procedures.

The textural structure of La–M (M = Mn, Fe, Co, and Ni) nanocomposites after the complete extraction of ionic liquids was carefully examined by N_2 sorption and transmission electron microscopy (TEM). The surface areas of La–M (M = Mn, Fe, Co, and Ni) derived from $[Bmim]^+Tf_2N^-$ media were determined to be 382, 505, 278 and 353 $m^2\ g^{-1}$, respectively, indicating that abundant nanopores were successfully incorporated into the lanthanum–M matrix (Table S1, ESI†). As expected, the N_2-sorption isotherms and their corresponding Barrett–Joyner–Halenda (BJH) adsorption pore size distribution curves are closely dependent on the M species, owing to the difference in the electrostatic $S^+X^-I^+$ interaction (Fig. 1a and b). For example, a transitional type of isotherm curve between typical I and IV curves was observed for La–Mn and La–Fe, corresponding to a pore size distribution at the microscale; whereas a representative type IV curve with an evident capillary condensation step with a relative pressure of 0.5–0.8 was discovered for La–Co and La–Ni, corresponding to BJH pore sizes of 5 and 7 nm, respectively. In Fig. 1c–f, abundant wormlike nanopores in the La–M matrix are clearly imaged by TEM, in good agreement with the N_2-sorption results.

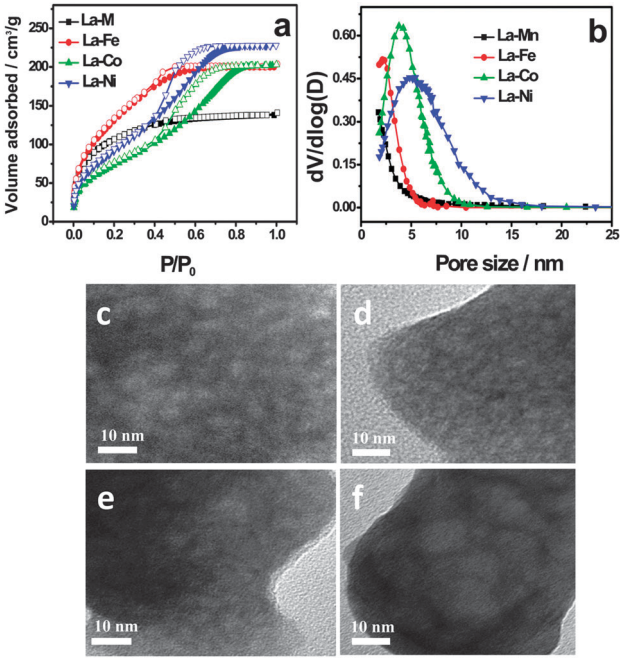

Fig. 1 Characterization of as-made La–Mn, La–Fe, LaCo, and La–Ni nanocomposites by using the ionic liquid $[Bmim]^+Tf_2N^-$. (a) N_2 sorption isotherms of La–M nanocomposites; (b) BJH adsorption pore-size distributions of La–M nanocomposites; (c–f) TEM images of La–Mn, La–Fe, La–Co and La–Ni nanocomposites.

The structural evolution of La–Mn nanocomposites under thermal treatment at different temperatures (400, 600, and 700 °C) was monitored by N_2 sorption isotherms, X-ray diffraction (XRD) patterns, Fourier-transform infrared (FTIR) spectra, and TEM images. When the heating temperature reached 400 °C, thermal decomposition of the inorganic species occurred (Fig. 2d), resulting in the significant transformation of the N_2-isotherm to a typical IV curve with an obvious H_2-type hysteresis loop (Fig. 2a). Correspondingly, its BJH pore size increased from the microscale to 4 nm, clearly demonstrating the formation of mesopores in the La–Mn matrix (Fig. 2b). Further increasing the heating temperature to 600 °C induced the crystallization of $LaMnO_3$ perovskite (Fig. 2c), and a well-crystallized $LaMnO_3$ perovskite was obtained at 700 °C treatment (Fig. 2c and d). The textural data (surface area and BJH pore size) for $LaMnO_3$ perovskite were determined to be 35 $m^2\ g^{-1}$ and 11 nm for the sample treated at 600 °C and 24 $m^2\ g^{-1}$ and 14 nm for the sample treated at 700 °C. The results indicate that mesoporous frameworks were indeed present in the $LaMnO_3$ perovskite matrix. The TEM images in Fig. 2e–g display the porous evolution in the nanodomains, in which wormlike mesoporous structures with abundant cavities are clearly observed. Textural and crystallization information for other $LaMO_3$ (M = Fe, Co, and Ni) perovskites treated at 650 °C is provided in Fig. S2 (ESI†). The surface areas and BJH pore sizes of $LaFeO_3$, $LaCoO_3$, and $LaNiO_3$ were determined to be 20 $m^2\ g^{-1}$ and 20 nm, 27 $m^2\ g^{-1}$ and 8 nm, and 21 $m^2\ g^{-1}$ and 9 nm, respectively (Table S1, ESI†).

As is well known, the self-assembly process involving the metal organic salt is closely dependent on the amount of water

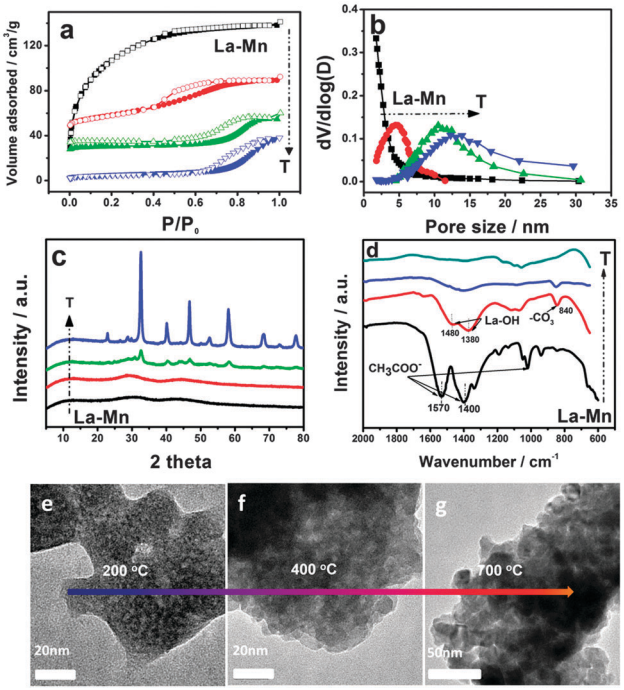

Fig. 2 Characterization of La–Mn calcinated at different temperatures. (a) N_2 sorption isotherms of La–Mn (■) and La–Mn nanocomposites calcinated at 400 °C (●, shift up for 40 cm^3 g^{-1}), 600 °C (▲, shift up for 20 cm^3 g^{-1}); 700 °C (▼), (b) BJH adsorption pore-size distributions of La–Mn and calcined La–Mn; (c) XRD patterns of La–Mn and calcined La–Mn; (d) FTIR patterns of La–Mn and calcined La–Mn; (e–g) high-resolution TEM images of $LaMnO_3$ calcinated at 200, 400, and 700 °C.

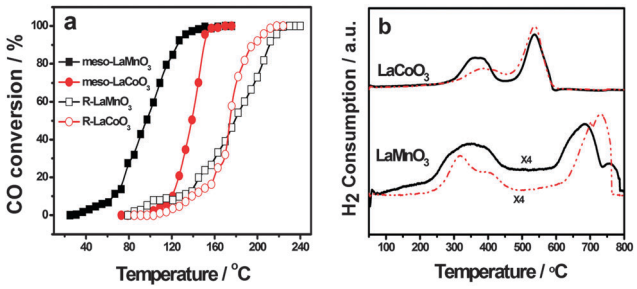

Fig. 3 Characterization of activities and redox of meso-$LaMnO_3$, R-$LaMnO_3$, (calcinated at 700 °C) and meso-$LaCoO_3$, R-$LaCoO_3$ (calcinated at 650 °C) perovskites. (a) Light-off curves of CO oxidation on mesoporous and bulk $LaMnO_3$ and $LaCoO_3$ (GHSV = 20 000 mL (h gcat)$^{-1}$); (b) H_2-TPR curves of meso-$LaMnO_3$ and meso-$LaCoO_3$ (black solid lines), R-$LaMnO_3$ and R-$LaCoO_3$ (red dotted lines).

added, which affects the initial hydrolysis and condensation of LMEO. Fig. S3 (ESI†) displays the N_2-sorption isotherms of La–Mn nanocomposites synthesized using different amounts of water in the precursor solution. It is interesting that microporous La–Mn nanocomposites with high surface areas of >350 m^2 g^{-1} can be synthesized under H_2O/La (mol) in the wide range of 0 to 8, which means hydrolysis and self-assembly in this process do not require severe synthesis conditions (*e.g.*, humidity, temperature, and pressure). Excessive hydrolysis occurs only when the ratio of H_2O to lanthanum is more than 12, which results in failure of self-assembly and a sharp decrease in the surface area.

The other remarkable advantage of the ionic liquid-mediated synthetic approach is that by simply changing the cation (S^+) molecule size of the ionic liquid, the pore structure of the La-M nanocomposites can also be easily adjusted. Taking the La–Mn nanocomposite as an example, as shown in the N_2-sorption isotherms and pore size distribution in Fig. S4 (ESI†), the La–Mn nanocomposites prepared by a protic $[N_{8,8,8,H}]^+Tf_2N^-$ ionic liquid all exhibit representative type IV curves with a sharp capillary condensation step in a relative pressure range of 0.7–0.9; these results indicate that larger pore sizes of 8–15 nm can be structured. More interestingly, the La–M nanocomposites with larger pore sizes prepared by $[N_{8,8,8,H}]^+Tf_2N^-$ show a more robust meso-scale porous framework, the surface area of which can reach 36 m^2 g^{-1} after heating at 700 °C. We believe that meso-$LaMO_3$ perovskites with higher surface areas could be synthesized using other potential ionic liquids.

The enlarged surface areas of the meso-$LaMO_3$ perovskites make them promising candidates for application in heterogeneous catalysis. Catalytic oxidation of CO is a typical gas–solid reaction that has been extensively studied because of its applications in many fields,[21] such as air purification, pollution control, and fuel cell technologies. Fig. 3a shows the catalytic performance toward CO oxidation of meso-$LaMnO_3$ and meso-$LaCoO_3$ perovskite samples prepared by $[Bmim]^+Tf_2N^-$. Performance data for bulk R-$LaMnO_3$ (7 m^2 g^{-1}) and R-$LaCoO_3$ (5 m^2 g^{-1}) prepared by the citrate sol–gel method are also included for comparison (for the N_2 sorption and XRD results of the samples see Fig. S5, ESI†). Among these materials, meso-$LaMnO_3$ and meso-$LaCoO_3$ show extremely high activity, and CO can be completely oxidized at 130 °C on meso-$LaMnO_3$ and at 150 °C on meso-$LaCoO_3$. Their catalytic activity is much higher than that of R-$LaMnO_3$ and R-$LaCoO_3$, which exhibit 95% conversion at temperatures above 220 and 210 °C, respectively. The meso-$LaMnO_3$ material was selected for long-term durability testing. The catalyst maintained 100% conversion, and no activity loss was observed for a consecutive 30 h at 140 °C (Fig. S6, ESI†).

The redox properties of meso-$LaMnO_3$ and meso-$LaCoO_3$ were investigated by H_2-TPR technology (Fig. 3b). Two reduction peaks were found at low temperatures (200–500 °C) and at high temperatures (600–800 °C) for all samples. The reaction peak areas of meso-$LaMnO_3$ and meso-$LaCoO_3$ at low temperatures were almost two fold higher than those of R-$LaMnO_3$ and R-$LaCoO_3$. For meso-$LaMnO_3$, in particular, the reduction temperature begins from 100 °C, which is quite consistent with the temperature of CO oxidation. In addition, the total H_2 consumption levels of mesoporous materials are higher than those of their corresponding bulk counterparts. This indicates that the pore structure and stoichiometric ligand assembly of lanthanum and the transition metal not only dramatically promote redox performance by increasing the amount of active oxygen but also increase the ratio of the transitional metal with a high valency, both of which are highly beneficial for heterogeneous catalytic oxidation reactions.

In summary, an ionic liquid-mediated synthetic strategy has been firmly established for the preparation of meso-$LaMO_3$

perovskites with robust crystalline frameworks. It takes advantage of the excellent thermal stability of ionic liquids to tightly crosslink the metal-containing species at high temperatures to construct a stable nanocomposition for nanotexture engineering. The high flexibility and compatibility of such synthetic strategies enable broad tunablity of ionic liquids and metal precursors for the preparation of other kinds of perovskites. Benefiting from the pore structure and La–M ligand assembly, the resulting meso-$LaMO_3$ exhibits extremely high activity and stability for CO oxidation. We believe the synthesis strategy reported here may open up new opportunities for preparing functional mesoporous complex mixed oxides of various compositions.

This work was supported by the U.S. Department of Energy, Office of Science, Basic Energy Sciences, Chemical Sciences, Geosciences, and Biosciences Division, the Natural Science Foundation of China (No. 21107096). HL and YC were supported in part by the Natural Science Foundation of Zhejiang province (No. LY14E080008) and the Commission of Science and Technology of Zhejiang province (No. 2013C03021).

Notes and references

1 (*a*) Y. Liu, H. Dai, J. Deng, L. Zhang, B. Gao, Y. Wang, X. Li, S. Xie and G. Guo, *Appl. Catal., B*, 2013, **140**, 317; (*b*) C. H. Kim, G. S. Qi, K. Dahlberg and W. Li, *Science*, 2010, **327**, 1624; (*c*) Y. Nishihata, J. Mizuki, T. Akao, H. Tanaka, M. Uenishi, M. Kimura, T. Okamoto and N. Hamada, *Nature*, 2002, **418**, 164; (*d*) S. Royer, D. Duprez, F. Can, X. Courtois, C. Batiot-Dupeyrat, S. Laassiri and H. Alamdari, *Chem. Rev.*, 2014, **114**, 10292.

2 (*a*) S. Pokhrel, L. H. Huo, H. Zhao and S. Gao, *Sens. Actuators, B*, 2007, **122**, 321; (*b*) M. M. Natile, A. Ponzoni, I. Concina and A. Glisenti, *Chem. Mater.*, 2014, **26**, 1505.

3 (*a*) L. M. Petkovic, V. Utgikar and S. N. Rashkeev, *J. Phys. Chem. C*, 2011, **115**, 8709; (*b*) X. Chen and S. P. Jiang, *J. Mater. Chem. A*, 2013, **1**, 4871; (*c*) A. A. Yaremchenko, V. V. Kharton, V. A. Kolotygin, M. V. Patrakeev, E. V. Tsipis and J. C. Waerenborgh, *J. Power Sources*, 2014, **249**, 483.

4 J. T. Mefford, W. G. Hardin, S. Dai, K. P. Johnston and K. J. Stevenson, *Nat. Mater.*, 2014, **13**, 726.

5 M. A. Pena and J. L. G. Fierro, *Chem. Rev.*, 2001, **101**, 1981.

6 (*a*) S. H. Liang, T. G. Xu, F. Teng, R. L. Zong and Y. F. Zhu, *Appl. Catal., B*, 2010, **96**, 267; (*b*) J. A. Villoria, M. C. Alvarez-Galvan, S. M. Al-Zahrani, P. Palmisano, S. Specchia, V. Specchia, J. L. G. Fierro and R. M. Navarro, *Appl. Catal., B*, 2011, **105**, 276.

7 (*a*) F. Teng, W. Han, S. H. Liang, B. G. Gaugeu, R. L. Zong and Y. F. Zhu, *J. Catal.*, 2007, **250**, 1; (*b*) N. A. Merino, B. P. Barbero, P. Ruiz and L. E. Cadus, *J. Catal.*, 2006, **240**, 245.

8 (*a*) G. J. Zou, L. Chen and X. L. Wang, *Catal. Lett.*, 2009, **127**, 444; (*b*) Z. Sarshar, F. Kleitz and S. Kaliaguine, *Energy Environ. Sci.*, 2011, **4**, 4258.

9 (*a*) X. C. Wang, J. C. Yu, Y. D. Hou and X. Z. Fu, *Adv. Mater.*, 2005, **17**, 99; (*b*) T. Y. Ma, Y. Zheng, S. Dai, M. Jaroniec and S. Z. Qiao, *J. Mater. Chem. A*, 2014, **2**, 8676.

10 (*a*) Y. X. Wang, X. Z. Cui, Y. S. Li, Z. Shu, H. R. Chen and J. L. Shi, *Microporous Mesoporous Mater.*, 2013, **176**, 8; (*b*) M. M. Nair, F. Kleitz and S. Kaliaguine, *ChemCatChem*, 2012, **4**, 387; (*c*) Y. G. Wang, J. W. Ren, Y. Q. Wang, F. Y. Zhang, X. H. Liu, Y. Guo and G. Z. Lu, *J. Phys. Chem. C*, 2008, **112**, 15293.

11 A.-H. Lu and F. Schueth, *Adv. Mater.*, 2006, **18**, 1793.

12 R. Zhang, P. Li, N. Liu, W. Yue and B. Chen, *J. Mater. Chem. A*, 2014, **2**, 17329.

13 (*a*) C. J. Brinker, Y. F. Lu, A. Sellinger and H. Y. Fan, *Adv. Mater.*, 1999, **11**, 579; (*b*) A. S. Poyraz, C.-H. Kuo, S. Biswas, C. K. King'ondu and S. L. Suib, *Nat. Commun.*, 2013, **4**, 2952; (*c*) T. Brezesinski, M. Groenewolt, A. Gibaud, N. Pinna, M. Antonietti and B. M. Smarsly, *Adv. Mater.*, 2006, **18**, 2260.

14 R. Chao, R. Munprom, R. Petrova, K. Gerdes, J. R. Kitchin and P. A. Salvador, *J. Am. Ceram. Soc.*, 2012, **95**, 2339.

15 (*a*) Z. Y. Zhang, G. M. Veith, G. M. Brown, P. F. Fulvio, P. C. Hillesheim, S. Dai and S. H. Overbury, *Chem. Commun.*, 2014, **50**, 1469; (*b*) J. S. Lee, X. Q. Wang, H. M. Luo and S. Dai, *Adv. Mater.*, 2010, **22**, 1004; (*c*) X. Q. Wang and S. Dai, *Angew. Chem., Int. Ed.*, 2010, **49**, 6664.

16 E. R. Cooper, C. D. Andrews, P. S. Wheatley, P. B. Webb, P. Wormald and R. E. Morris, *Nature*, 2004, **430**, 1012.

17 (*a*) S. Dai, Y. H. Ju, H. J. Gao, J. S. Lin, S. J. Pennycook and C. E. Barnes, *Chem. Commun.*, 2000, 243; (*b*) B. G. Trewyn, C. M. Whitman and V. S. Y. Lin, *Nano Lett.*, 2004, **4**, 2139; (*c*) Y. Zhou, J. H. Schattka and M. Antonietti, *Nano Lett.*, 2004, **4**, 477.

18 (*a*) S. H. Zhou, Z. Ma, G. A. Baker, A. J. Rondinone, Q. Zhu, H. M. Luo, Z. L. Wu and S. Dai, *Langmuir*, 2009, **25**, 7229; (*b*) Y. Zhou and M. Antonietti, *J. Am. Chem. Soc.*, 2003, **125**, 14960.

19 (*a*) A. Taubert and Z. Li, *Dalton Trans.*, 2007, 723; (*b*) Z. Ma, J. H. Yu and S. Dai, *Adv. Mater.*, 2010, **22**, 261; (*c*) M. Antonietti, D. B. Kuang, B. Smarsly and Z. Yong, *Angew. Chem., Int. Ed.*, 2004, **43**, 4988; (*d*) R. E. Morris, *Chem. Commun.*, 2009, 2990.

20 (*a*) Z. Hu and C. J. Margulis, *Acc. Chem. Res.*, 2007, **40**, 1097; (*b*) Z. H. Hu and C. J. Margulis, *Proc. Natl. Acad. Sci. U. S. A.*, 2006, **103**, 831; (*c*) A. Mele, C. D. Tran and S. H. D. Lacerda, *Angew. Chem., Int. Ed.*, 2003, **42**, 4364.

21 (*a*) P. Venkataswamy, K. N. Rao, D. Jampaiah and B. M. Reddy, *Appl. Catal., B*, 2015, **162**, 122; (*b*) P. Xiao, J. Zhu, H. Li, W. Jiang, T. Wang, Y. Zhu, Y. Zhao and J. Li, *ChemCatChem*, 2014, **6**, 1774; (*c*) S. J. Huang, K. Hara and A. Fukuoka, *Energy Environ. Sci.*, 2009, **2**, 1060.

